Feasibility of Geophysical Monitoring of Carbon-Sequestrated Deep Saline Aquifers

Final Scientific Report

Report period start date: *October 2009*
Report period end date: *September 2013*

Principal Authors
Project Director Subhashis Mallick
Co-Project Director Vladimir Alvarado

Date: March 20, 2014

DOE Award No: DE-FE0001160

Submitting Organization

University of Wyoming, Office of Research

1000 E. University Ave, Laramie, WY 82071, USA

DISCLAIMER

ABSTRACT

As carbon dioxide (CO_2) is sequestered from the bottom of a brine reservoir and allowed to migrate upward, the effects of the relative permeability hysteresis due to capillary trapping and buoyancy driven migration tend to make the reservoir patchy saturated with different fluid phases over time. Seismically, such a patchy saturated reservoir induces an effective anisotropic behavior whose properties are primarily dictated by the nature of the saturation of different fluid phases in the pores and the elastic properties of the rock matrix. By combining reservoir flow simulation and modeling with seismic modeling, it is possible to derive these effective anisotropic properties, which, in turn, could be related to the saturation of CO_2 within the reservoir volume any time during the post-injection scenario. Therefore, if time-lapse seismic data are available and could be inverted for the effective anisotropic properties of the reservoir, they, in combination with reservoir simulation could potentially predict the CO_2 saturation directly from the time-lapse seismic data. It is therefore concluded that the time-lapse seismic data could be used to monitor the carbon sequestrated saline reservoirs. But for its successful implementation, seismic modeling and inversion methods must be integrated with the reservoir simulations. In addition, because CO_2 sequestration induces an effective anisotropy in the sequestered reservoir and anisotropy is best detected using multicomponent seismic data compared to single component (P-wave) data, acquisition, processing, and analysis is multicomponent seismic data is recommended for these time-lapse studies. Finally, a successful implementation of using time-lapse seismic data for monitoring the carbon sequestrated saline reservoirs will require development of a robust methodology for inverting multicomponent seismic data for subsurface anisotropic properties.

TABLE OF CONTENTS

EXECUTIVE SUMMARY

In this project we used synthetic examples and combined reservoir flow simulation with seismic modeling and inversion to successfully demonstrate the feasibility of time lapse monitoring of the carbon dioxide (CO_2) sequestrated deep saline reservoirs. Our simulation modeling demonstrated that as CO_2 is sequestered into a realistic saline reservoir, and allowed to migrate, fully considering the effect of the relative permeability hysteresis due to capillary trapping and buoyancy driven migration, the reservoir tends to become patchy saturated with different fluid phases over time. Extracting reservoir saturation models at different times after sequestration and computing the elastic models using Gassmann fluid substitution, we also demonstrated these patchy-saturated models are seismically anisotropic in nature and could be effectively modeled by replacing the entire reservoir rock by a stack of equivalent or effective azimuthally anisotropic layers. We also demonstrated that the elastic properties of these equivalent anisotropic layers including density can predict the CO_2 saturation within the reservoir volume to a reasonable accuracy at any time during the post-injection scenario. Therefore, if time lapse seismic data from CO_2 sequestration sites are available, an anisotropic waveform inversion could potentially extract the equivalent anisotropic models, which, in turn, could predict saturation and the totality of CO_2 during the post-injection periods. We went further and developed a prestack waveform inversion methodology for azimuthally anisotropic media using a multi-objective, multi-component, and multi-scale optimization methodology which could be used for extracting anisotropic properties and density from time lapse seismic data and predict CO_2 saturation. We conclude that the time-lapse monitoring of the carbon sequestrated deep saline aquifers is feasible but it requires combining seismic modeling and inversion with the reservoir flow simulation. Additionally, because CO_2 sequestered reservoirs tend to become seismically anisotropic and anisotropy is best detected from multicomponent seismic data, it is mandatory that we use multicomponent not the single-component seismic data for such time lapse monitoring and accurate prediction of the CO_2 storage within the sequestered reservoir volumes.

INTRODUCTION AND THE SCIENTIFIC QUESTIONS ADDRESSED

As the fossil-fuels are likely to contribute a major portion of the energy-basket in the foreseeable future, the effects of greenhouse gas emissions from the fossil-fuel burnings is a major concern to the environment. The most viable solution to reduce these emissions is carbon capture and storage. Over the past decade, the US Department of Energy (DOE) spent considerable amount research dollars towards this initiative. Although capturing CO_2 and sequestering them into the depleted hydrocarbon and deep saline reservoirs with an impermeable seal on top is a natural choice for carbon storage, a lot of issues must be addressed to ensure its safety. It is important to ensure that the sequestered CO_2 does not disturb the geological integrity of the surrounding rock

formations and are permanently stored within the sequestered reservoir volumes. It is also important that the CO_2 does not does not disturb the in-situ stress conditions such that the overburden seal rocks are fractured causing leakage pathways for the CO_2 to escape back into the atmosphere and/or contaminate the fresh groundwater that could potentially be used for drinking. To address these fundamental issues, remote monitoring of the sequestered reservoir volumes is essential.

Our project is based on the feasibility of such a monitoring and attempted to address the following scientific questions:

1. What is the most cost-effective way to monitor CO_2 sequestrated reservoirs?
2. Is it possible to ensure that the CO_2 is safely stored without disturbing the geological integrity of the surrounding rock formations?
3. Is it possible to quantify the totality of the sequestered CO_2 at any time during the post-injection scenario?

PROJECT RESULTS

In a modeling study of synthetic CO_2 sequestration scenario into a realistic reservoir, Behzadi et al. (2011) and Padhi et al. (2014) combined reservoir simulation with seismic modeling with full consideration of the impact of relative permeability hysteresis and capillary trapping on buoyancy driven migration and found the following:

- As CO_2 is sequestered into a saline reservoir and is allowed to migrate upward, it tends to exhibit a patchy saturation of different fluid phases over time.
- Computing the exact patchy saturated heterogeneous elastic model from simulation using Gassmann fluid substitution (Mavko et al., 1998) at different times after sequestration, and computing the seismic responses for those models using a finite-difference modeling, Padhi et al. (2014) also found that
    - Seismically, the heterogeneous model of the reservoir could be replaced by a stack of homogeneous and "effective" anisotropic layers.
    - The properties of the effective anisotropic layers including density can also predict the CO_2 saturation within the reservoir during any phase of the post-injection scenario to reasonable accuracy.
- Figures 1 and 2 below summarize the result of this synthetic study.

The results, shown in Figures 1 and 2 demonstrate the following facts:

1. If time-lapse seismic data from the CO_2 sequestration sites are available, they are likely to behave anisotropically over the sequestered reservoir interval during all periods after the CO_2 injection.
2. The anisotropic properties and density over the sequestered reservoir interval if extracted, they could be combined with the reservoir simulation and be used to predict CO_2 saturation and hence the totality of the stored CO_2 within the reservoir during all post-injection periods.

3. Because anisotropic properties and density are best detected from multicomponent seismic data, it is necessary that we acquire multicomponent data for such time lapse analyses.
4. Although the results shown in Figures 1 and 2 are related to CO_2 sequestrated reservoirs, the apparent anisotropic behavior is also true for other types of reservoirs:
    a. Unconventional reservoirs are inherently anisotropic and the same methodology outlined above could be used to characterize them.
    b. During production from a conventional reservoir, the evolving patchy saturation of different fluids will cause the emergence of a time-dependent anisotropy. Therefore, the extraction of equivalent anisotropic properties from time lapse seismic data during the phases of enhanced oil recovery could potentially identify the patches of bypassed hydrocarbons.

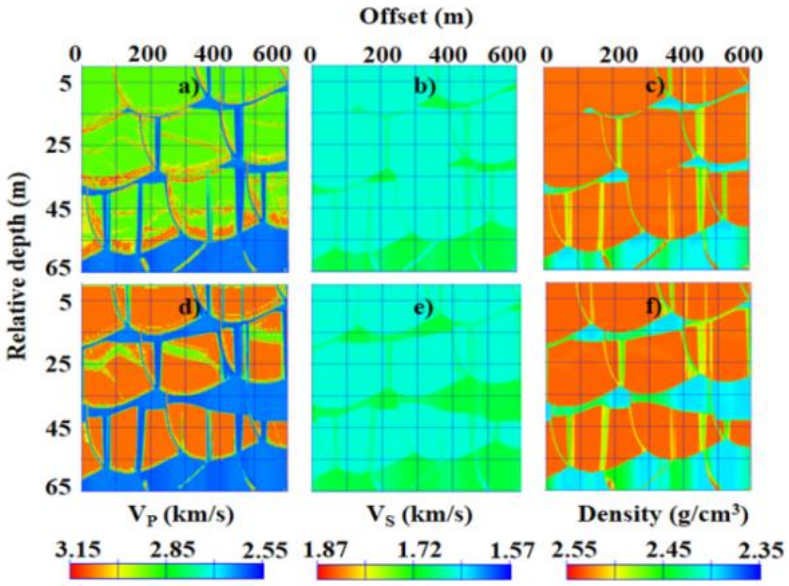

Figure 1: *Synthetic reservoir modeling experiment of CO_2 sequestration in a realistic eolian saline reservoir. (a)-(c) P and S-wave velocity (V_P, V_S) and density model five years after sequestration and (d)-(f) the same fifty-five years after sequestration (After Padhi et al., 2014).*

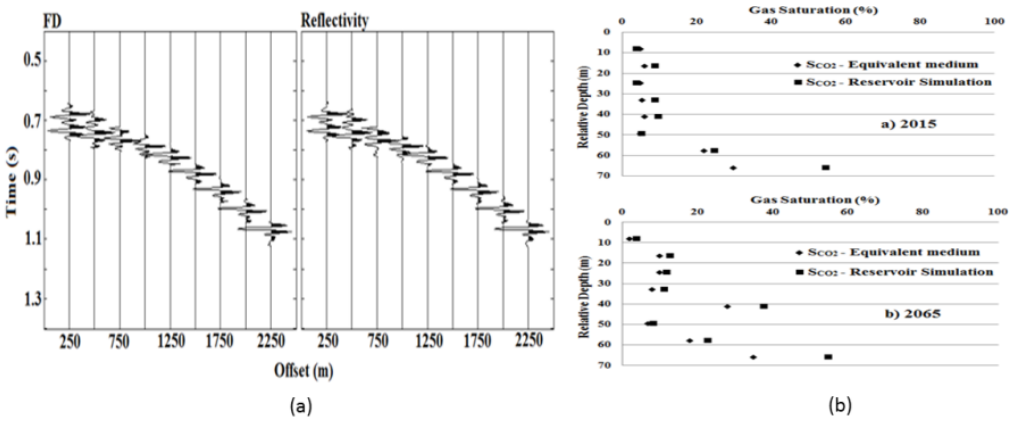

Figure 2: *(a) Comparison of seismic simulation of the reservoir model fifty-five years after CO_2 sequestration using the exact model and finite-difference (FD) simulation with the one where the model is replaced by a stack of homogeneous anisotropic layers and an anisotropic reflectivity modeling is used to compute synthetics. (b) Comparison of actual and predicted CO_2 saturation five (2015) and fifty-five (2065) years after CO_2 sequestration using the effective anisotropic model (After Padhi et al., 2014).*

The modeling studies outlined in Figures 1 and 2 demonstrate that if the time-lapse seismic data are inverted for the equivalent anisotropic properties and density of the reservoir, they when combined with the reservoir simulation could potentially predict the totality of the injected CO_2 within the reservoir volumes. In addition, the potential application of this method is beyond CO_2 sequestered reservoirs and is applicable to characterizing the unconventional hydrocarbon reservoirs and during the enhanced recovery phases from the conventional hydrocarbon reservoirs. Success of such methodology will however depend on extracting the subsurface anisotropic properties and density from seismic data. In past studies, it has been demonstrated that under the isotropic assumptions, density could be more reliably extracted from multicomponent seismic data than from the traditional single component (P-wave) data (Mallick, 2000). This is due to the fact that the mode-converted reflections recorded in multicomponent data are more sensitive to density at small reflection angles that the primary P-wave reflections (Aki and Richards, 2002). In addition, because S-waves are more sensitive to anisotropy than the P-waves (Thomsen, 1988), an accurate extraction of subsurface anisotropy requires multicomponent data. It is therefore necessary to acquire time lapse multicomponent seismic data to accurately monitor the CO_2 sequestrated reservoirs. In addition, any inversion methodology for extracting subsurface anisotropic properties and density from multicomponent seismic data must also be able to estimate the uncertainty associated with each parameter estimate, so that when combined with the reservoir simulation, we can not only quantify CO_2 saturation and its totality, but also the uncertainty associated with our estimates.

Development of an anisotropic waveform inversion of multicomponent seismic data is however a challenge. Note that multicomponent data has multiple objectives, one for each data component. Typically, such multiobjective problems are handled by defining a single objective given as a

weighted sum of the objectives of different data components (Mallick, 2000; Chang and McMechan, 2009) and sometimes with additional regularization terms (Du and MacGregor, 2010; Karaoulis et al, 2012) which is then followed by a single objective optimization. Although such an approach has yielded good results on synthetic data (for example, see Mallick, 2000; Chang and McMechan, 2009), Padhi and Mallick (2013a, b) pointed out some fundamental drawbacks of such an approach. All multiobjective problems are nonlinear with nonunique solutions, known as the Pareto-optimal solutions, none of which could be considered the best (Deb et al., 2002). Defining multiple such objectives as a single one can provide only a single solution out of the entire Pareto-optimal set, which could be biased by the choice of the individual weights. The entire Pareto-set could be obtained by changing weights and inverting repeatedly, but it is too cumbersome and computationally inefficient. A more efficient approach would be to treat the entire set of objectives as a vector and simultaneously invert all its components.

In this project, we used such an approach using a fast nondominated sorting genetic algorithm or NSGA-II (Deb et al., 2002) to successfully invert two component (primary or P-P and mode-converted or P-SV) synthetic seismic data for the most simple type of anisotropy known as the transverse isotropy with a vertical symmetry axis (VTI) (Padhi and Mallick 2013a, b). Figure 3 shows the inversion result of Padhi and Mallick (2013b). Note from Figure 3 that in addition to reasonably estimating the anisotropic parameters, the inversion could also estimate the Pareto-optimal set of solutions (Figure 3f). These Pareto-optimal solutions, stored in the model space was, in turn, used to estimate the a-posteriori probability density distribution of each model parameter, providing not only the most optimal model, but also an estimate of the uncertainty associated with each parameter estimate (Figure 3g). Li and Mallick (2013) extended the work of Padhi and Mallick (2013a, b) further to invert three-component seismic data along two azimuths, i.e. for a total of six objectives, for more general forms of anisotropy such as transverse isotropy with a horizontal symmetry axis (HTI) and orthorhombic (ORT) media (Figure 4).

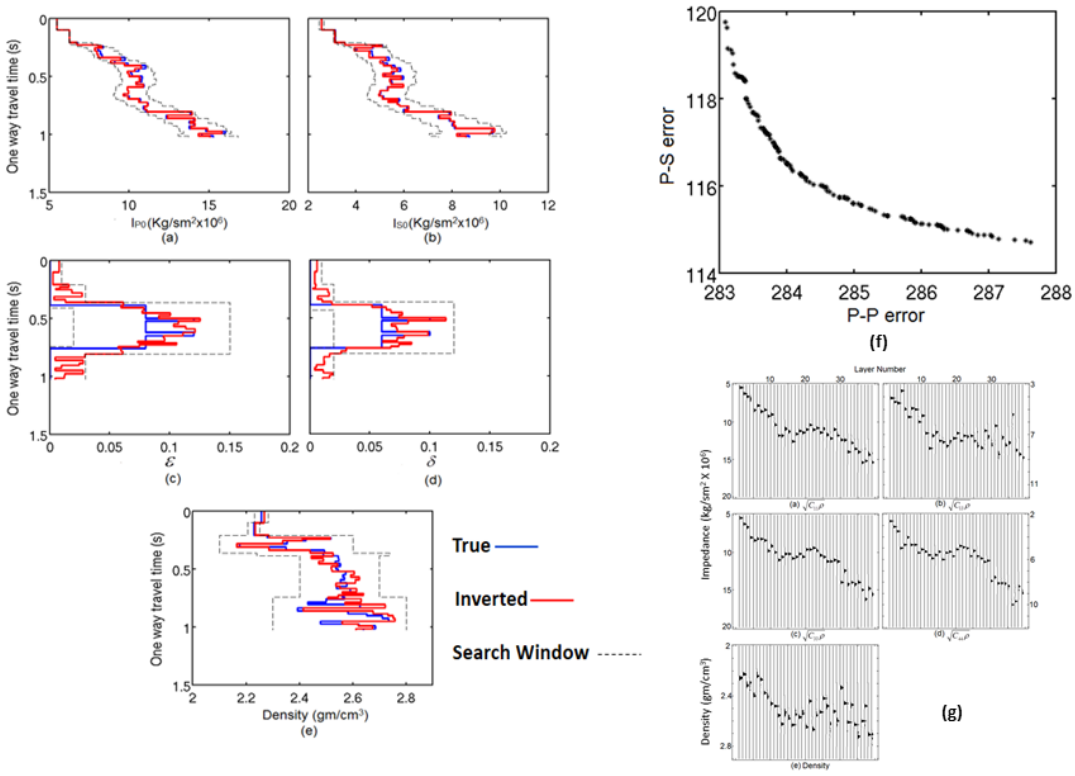

Figure 6: *Two-component seismic inversion for VTI media parameters. (a)-(e) Comparison of true and inverted models and the search bounds used in inversion. (f) One set of Pareto-optimal solution. Note that none of the solutions shown are better than one another in terms of satisfying both objectives, i.e., minimizing both P-P and P-S errors. In multiobjective optimization, they are called nondominating solutions and they belong to the same Pareto-front or rank. In fact, there are multiple such Pareto-fronts, all of which could then be combined to get an estimate of the a-posteriori probability density (PPD) in the model space as shown in (g). Such a PPD not only allows estimating the optimal solution, but it also allows estimating the uncertainty associated with the estimation of each model parameter. See Padhi and Mallick (2013b) for details.*

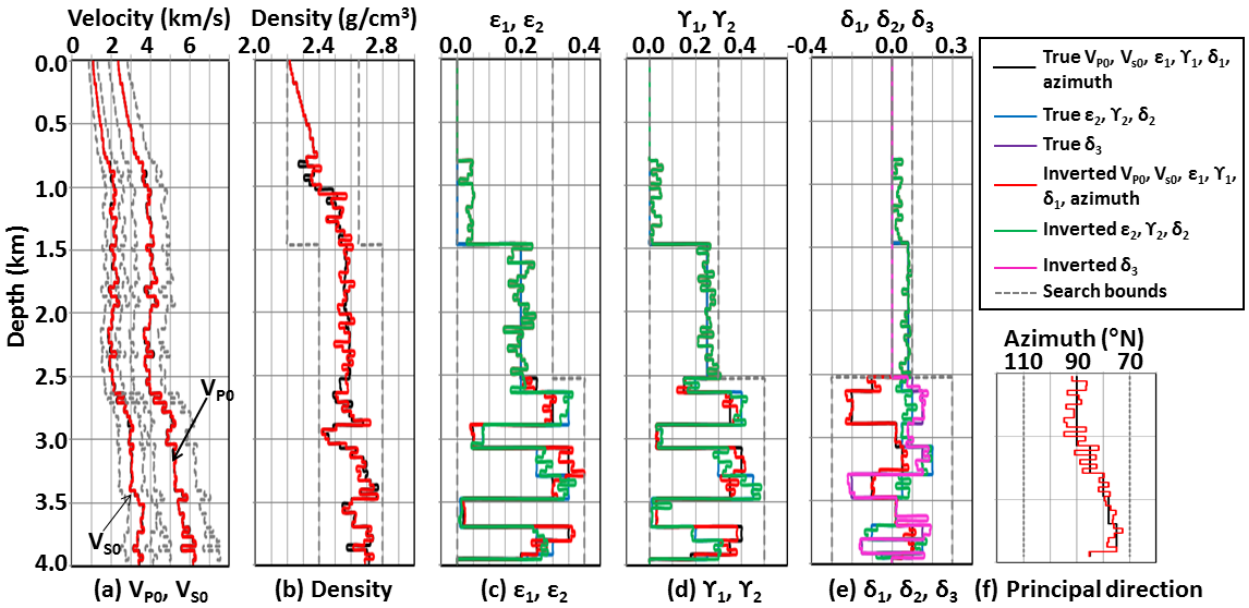

Figure 4: *Inversion of 3 component/two azimuth synthetic seismic data for orthorhombic media parameters compared with the true model. The velocity and density of the model is based on the Rock-Springs uplift (RSU) well data and additional anisotropic properties were added from 1.5 km and below. (a) Inverted vertical P- and S-wave velocities (V_{P0}, V_{S0}). (b) Inverted density. (c) Inverted anisotropy parameters ε_1 and ε_2. (d) Inverted anisotropy parameters γ_1 and γ_2 (e) Inverted anisotropy parameters δ_1, δ_2, δ_3. (f) Principal anisotropy direction. The search bounds used for inversion are shown as dashed lines. Note that the true model is isotropic up to 1.5 km ($\varepsilon_1 = \varepsilon_2 = \Upsilon_1 = \Upsilon_2 = \delta_1 = \delta_2 = \delta_3 = 0$). Between 1.5-2.5 km it is VTI ($\varepsilon_1 = \varepsilon_2$; $\gamma_1 = \gamma_2$, $\delta_1 = \delta_2$, and $\delta_3 = 0$). Finally, it is azimuthally anisotropic (HTI and ORT) below 2.5 km. For the azimuthally anisotropic part of the model, there is a thin HTI layer right below 2.5 km, and the rest is ORT. Note that not only the extracted properties are reasonably accurate, but the inversion converged to the correct anisotropic symmetries of the true model. The anisotropic parameters are the Thomsen-Tsvankin parameters (Thomsen, 1986; Tsvankin, 1997).*

In this project, not only we combined reservoir simulation with seismic modeling and demonstrated the feasibility of monitoring the carbon sequestrated deep saline reservoirs, but we also developed a practical methodology for inverting multicomponent seismic data that could be effectively used for such monitoring. We therefore addressed all three fundamental research questions (see above) in our study.

SUGGESTIONS FOR FUTURE WORK

The feasibility study outlined in this work was based purely on synthetic data. In combining reservoir simulation with seismic modeling, we used realistic reservoir models (Behzadi et al, 2011; Padhi et al, 2014). In demonstrating the anisotropic inversion methodology also, we used synthetic data based on real well logs (Padhi and Mallick, 2013a, b; Li and Mallick, 2013). Additionally, we also tested the accuracy of our inversion in the presence of noise (Padhi and

Mallick, 2013b). It is however necessary to go beyond these synthetic experiments and demonstrate our workflow on real data. In addition, while combining reservoir simulation with seismic modeling although the pressure effects at grid scale were accounted for in the simulation runs, the resultant equivalent anisotropy was completely attributed to the patchy saturated fluids. In reality, the additional pressure resulting from CO_2 injection is likely to alter the in-situ stress fields within the reservoirs and the surrounding rock formations that may induce additional anisotropy. Separating this stress-induced anisotropy from the one caused from the patchy fluid saturation is important. For example, if this induced stress field fractures the reservoir rock, we would like to monitor it because it is may further enhance CO_2 storage. At the same time, we must also ensure these stress fields do not induce fractures in the overlying seals providing leakage pathways for CO_2 to escape. Characterization of the anisotropy caused from the stress fields and the one from the patchy-saturated distribution of fluid phases will require enhancements to both flow simulation and seismic modeling used in our current study. Flow simulations must be coupled with geomechanical modeling and analysis into a coupled simulation/geomechanics workflow. Additionally, the seismic modeling and inversion used in our current study was purely based on elastic anisotropic assumptions which did not take the effect of the fluid-pore interactions into account. These fluid-pore interaction could however be incorporated into the algorithm using Biot's theory and Darcy's law into a poro-elastic modeling algorithm (Biot, 1956, 1962). Such a coupled simulation/geomechanics workflow in conjunction with seismic inversion based on poro-elasticity will be capable of accurately predicting the porosity, fluid saturation, and stress fields within the reservoir and its surroundings. Such a methodology would not only allow accurate estimation of the stored CO_2 but also it will provide information on the leakage pathways through which the stored fluid may escape. Multicomponent seismic data have been acquired at the Rock-Springs uplift (RSU), Wyoming under a separately funded DOE project (DE-FE-002142), primarily for site characterization of most promising reservoirs in this area for CO_2 sequestration. It would therefore be ideal to further develop our current work to include flow simulation coupled with geomechanics and poro-elastic theory and apply it to the RSU seismic data. We are currently trying to collaborate with the Oklahoma State University and preparing a detailed research proposal to take our current work further along these lines and apply to the RSU seismic data.

CONCLUSIONS

Time lapse seismic data is a highly effective tool for monitoring the CO_2 sequestrated saline reservoirs and predict the volume of the stored fluid after injection. This however requires that seismic modeling and inversion methods are combined with the reservoir simulation so that the effective strategies to predict fluid saturation directly from seismic data could be developed. CO_2 injection induces and effective or apparent anisotropy to the recorded seismic data. Because the anisotropy is better detected from multicomponent seismic data compared to P-wave data, we recommend multicomponent data acquisition for all CO_2 monitoring experiments. The methodology outlined in our study could further be improved by including geomechanical

component to the fluid flow simulation and poro-elasticity to the seismic modeling and inversion. Finally, although our current study was based on the CO_2 sequestrated reservoirs, our method is equally applicable for characterizing the unconventional reservoirs and the conventional reservoirs during enhanced oil recovery.

REFERENCES

Aki, K., and P.G. Richards, 2002, Quantitative Seismology: University Science Books.

Behzadi, H., V. Alvarado, and S. Mallick**,** 2011, CO_2 saturation, distribution, and seismic response in two dimensional permeability model: Environ. Sci. Technol., **45**, 9435-9441.

Biot, M.A., 1956, Theory of propagation of elastic waves in a fluid saturated porous solid. I. Low frequency range and II. Higher frequency range: J. Acoust. Soc. Am., **28**, 168-191.

Biot, M.A., 1962, Mechanics of deformation and acoustic propagation in porous media: J. Appl. Phys., **33**, 1482-1498.

Chang, H. and G. McMechan, 2009, 3D 3-C full-wavefield elastic inversion for estimating anisotropic parameters: A feasibility study with synthetic data: Geophysics, **74**, WCC159-WCC175.

Deb, K**.**, A. Pratap, S. Agarwal, and T. Meyarivan, 2002, A fast and elitist multi-objective genetic algorithm: NSGA-II: IEEE Transaction on Evolutionary Computation, **6(2)**, 181-197.

Du, Z., and L.M. MacGregor, 2010, Reservoir characterization from joint inversion of marine CSEM and seismic AVA data using Genetic Algorithms: a case study based on the Luva gas field: SEG Technical Program Expanded Abstracts, **29,** 737-741.

Karaoulis, M., A. Revil, J. Zhang, and D.D. Werkema, 2012, Time-lapse joint inversion of crosswell DC resistivity and seismic data: A numerical investigation: Geophysics, **77**, D141-D157.

Li, T., and S. Mallick, 2013, Prestack waveform inversion of four-component, two-azimuth surface seismic data for orthorhombic elastic media parameters using a nondominated sorting genetic algorithm: SEG Technical Program Expanded Abstracts, **32**, 3283-3287.

Mallick, S., 2000, Prestack waveform inversion of multicomponent seismic data: SEG Technical Program Expanded Abstracts, **19**, 2273-2276.

Mavko, G., T. Mukerji, and J. Dvorkin, 1998, The rock physics handbook: Cambridge University Press.

Padhi, A., and S. Mallick, 2013a, Accurate estimation of density from the inversion of multicomponent prestack seismic waveform data using a nondominated sorting genetic algorithm: The Leading Edge, **32**, 94-98.

Padhi, A., and Mallick, S., 2013b, Multicomponent prestack seismic waveform inversion in transversely isotropic media using a nondominated sorting genetic algorithm: Geophysical Journal International, doi: 10.1093/gji/ggt460.

Padhi, A., S. Mallick, H. Behzadi, and V. Alvarado, 2014, Efficient modeling of seismic signature of patchy saturation for time lapse monitoring of carbon sequestrated deep saline reservoirs: Applied Energy, **114**, 445-455.

Thomsen, L., 1986. Weak elastic anisotropy: Geophysics, **51**, 1954–1966.

Thomsen, L., 1988, Reflection seismology over azimuthally anisotropic media: Geophysics, **53**, 304-313.

Tsvankin, I., 1997. Anisotropic parameters and P-wave velocity for orthorhombic media: Geophysics, **62,** 1292–1309.

ACRONYMS/ABBREVIATIONS

CO_2: Carbon dioxide.
DOE: US Department of Energy.
HTI: Transversely isotropic medium with horizontal axis of symmetry.
ORT: Orthorhombic elastic medium.
RSU: Rock-Springs uplift.
V_P: P-wave velocity.
V_S: S-wave velocity.
VTI: Transversely isotropic medium with vertical axis of symmetry.

APPENDIX-A (Publications/presentations from the project)

Peer-reviewed journal publications

Behzadi, H., Alvarado, V., and Mallick, S., 2011, CO_2 saturation, distribution, and seismic response in two dimensional permeability model: Environ. Sci. Technol., **45**, 9435-9441.

Mukhopadhyay, P.K., and Mallick, S., 2011, An accurate ray-based offset-to-angle transform from normal moveout uncorrected multicomponent data in a transversely isotropic medium with vertical symmetry axis: Geophysics, **76**, C41-C51.

Padhi, A., and Mallick, S., 2013a, Accurate estimation of density from the inversion of multicomponent prestack seismic waveform data using a non-dominated sorting genetic algorithm: The Leading Edge, **32**, 94-98.

Padhi, A., and Mallick, S., 2013b, Multicomponent prestack seismic waveform inversion in transversely isotropic media using a non-dominated sorting genetic algorithm: Geophysical Journal International, doi: 10.1093/gji/ggt46.

Padhi, A., Mallick, S**.**, Behzadi H., and Alvarado, V., 2014, Efficient modeling of seismic signature of patchy saturation for time lapse monitoring of carbon sequestrated deep saline reservoirs: Applied Energy, **114**, 445-455.

Mukherjee, D., Mallick, S., Campbell-Stone, E., and Shaffer, L., 2014, Azimuthal anisotropy analysis of P-wave seismic data and estimation of the orientation of the in-situ stress fields- an example from the Rock-Springs uplift, Wyoming: Geophysics (under review).

Peer-reviewed expanded abstracts presented at conferences

Mukhopadhyay, P.K., and Mallick, S**.**, 2009, A new ray-based offset-to-angle transform for anisotropic medium and its implication in the prestack waveform inversion of seismic data: SEG Technical Program Expanded Abstracts, **28 (1)**, 321-325.

Mukhopadhyay, P.K., Mallick, S., Padhi, A., and Alvarado, V., 2010, Time-lapse monitoring carbon sequestrated brine acquifers- a feasibility study: SEG Technical Program Expanded Abstracts, **29 (1)**, 1630-1634.

Mallick, S., Mukhopadhyay, P.K., Padhi, A., and Alvarado, V., 2010, Prestack waveform inversion- the present state and the road ahead: SEG Technical Program Expanded Abstracts, **29 (1)**, 4428-4431.

Padhi, A., Mallick, S., Mukhopadhyay, P.K., Behzadi, H., and Alvarado, V., 2011, Seismic signature of a patch saturation and its implication to time-lapse monitoring of carbon-sequestrated deep saline reservoirs: SEG Technical Program Expanded Abstracts, **30 (1)**, 2287-2291.

Behzadi, H., Alvarado, V., Padhi, A., and Mallick, S., 2011, CO2 saturation, distribution and seismic response in 2D permeability model: SEG Technical Program Expanded Abstracts, **30 (1)**, 4207-4211.

Padhi, A., and Mallick, S., 2012, Multicomponent prestack waveform inversion for isotropic elastic media parameters using a non-dominated sorting genetic algorithm: SEG Expanded Abstracts, doi: 10.1190/segam2012-1331.1.

Padhi, A., and Mallick, S., 2012, Multicomponent prestack waveform inversion for VTI media parameters using a non-dominated sorting genetic algorithm: SEG Technical Program Expanded Abstracts, doi: 10.1190/segam2012-1340.1.

Mukherjee, D., Mallick, S., Shafer, L., and Campbell-Stone, E., 2012, Estimation of in-situ stress fields from P-wave seismic data: SEG Technical Program Expanded Abstract, doi: 10.1190/segam2012-0375.1.

Li, T., and Mallick, S., 2013, Prestack waveform inversion of four-component, two-azimuth surface seismic data for orthorhombic elastic media parameters using a nondominated sorting genetic algorithm: SEG Technical Program Expanded Abstracts, **32**, 3283-3287.

Padhi, A., and Mallick, S., 2013, Accurate estimation of VTI media parameters using multicomponent prestack waveform inversion: SEG Technical Program Expanded Abstracts, **32**, 1664-1668.

APPENDIX-B (Project progress by task)

Task #	Description	Planned % Complete	Actual % Complete
1	Project Management, Planning, and Reporting	100	100
2	3-D model generation	100	100
3	Inversion Development	100	100
4	Processing and Inversion	100	100

APPENDIX-C (Cost plan/status)

Budget Period 1

Baseline Reporting Quarter		Year 1	Start: 10/1/2009	End: 09/30/2010			
	10/01/09 - 12/31/09		01/01/10 - 03/30/10		04/01/10 - 06/30/10	07/01/10-09/30/10	
	Q1	Cumulative To	Q2	Cumulative To	Q3	Cumulative Total	Q4	Cumulative Total
Baseline Cost Plan								
(from SF 424A)								
Federal Share	$241,875.00	$241,875.00	$61,874.75	$303,749.75	$61,875.50	$365,625.25	$61,874.75	$427,500.00
Non-Federal Share	$52,110.25	$52,110.25	$36,137.25	$88,247.50	$36,310.25	$124,557.75	$36,310.25	$160,868.00
Total Planned (Federal and non-Federal)	$293,985.25	$293,985.25	$98,012.00	$391,997.25	$98,185.75	$490,183.00	$98,185.00	$588,368.00
Actual Incurred Cost								
Federal Share	$36,410.51	$36,410.51	$22,729.62	$59,140.13	$275,300.52	$334,440.65	$26,415.98	$360,856.63
Non-Federal Share	$0.00	$0.00	$0.00	$0.00	$0.00	$0.00	$0.00	$0.00
tal Incurred Costs Quarter (Federal and non-Federal)	$36,410.51	$36,410.51	$22,729.62	$59,140.13	$275,300.52	$334,440.65	$26,415.98	$360,856.63
Variance								
Federal Share	$205,464.49	$205,464.49	$39,145.13	$244,609.62	-$213,425.02	$31,184.60	$35,458.77	$66,643.37
Non-Federal Share	$52,110.25	$52,110.25	$36,137.25	$88,247.50	$36,310.25	$124,557.75	$36,310.25	$160,868.00
Total Variance Quarterly (Federal and non-Federal)	$257,574.74	$257,574.74	$75,282.38	$332,857.12	-$177,114.77	$155,742.35	$71,769.02	$227,511.37

Budget Period 2

		Year 2	Start: 10/1/2010			End: 09/30/2011	
10/01/10 - 12/31/10		01/01/11 - 03/30/11		04/01/11 - 06/30/11		07/01/11-09/30/11	
Q5	Cumulative Total	Q6	Cumulative Total	Q7	Cumulative Total	Q8	Cumulative Total
$164,460.00	$591,960.00	$64,459.00	$656,419.00	$64,459.00	$720,878.00	$64,459.00	$785,337.00
$41,482.00	$202,350.00	$41,482.00	$243,832.00	$41,481.00	$285,313.00	$41,482.00	$326,795.00
$205,942.00	$794,310.00	$105,941.00	$900,251.00	$105,940.00	$1,006,191.00	$105,941.00	$1,112,132.00
$7,129.22	$367,985.85	$19,867.91	$387,853.76	$62,309.72	$450,163.48	$145,924.99	$596,088.47
$0.00	$0.00	$287,421.63	$287,421.63	$9,158.86	$296,580.49	$0.00	$296,580.49
$7,129.22	$367,985.85	$307,289.54	$675,275.39	$71,468.58	$746,743.97	$145,924.99	$892,668.96
$157,330.78	$223,974.15	$44,591.09	$268,565.24	$2,149.28	$270,714.52	-$81,465.99	$189,248.53
$41,482.00	$202,350.00	-$245,939.63	-$43,589.63	$32,322.14	-$11,267.49	$41,482.00	$30,214.51
$198,812.78	$426,324.15	-$201,348.54	$224,975.61	$34,471.42	$259,447.03	-$39,983.99	$219,463.04

Budget Period 3

		Year 3	Start: 10/1/2011			End: 09/30/2012	
10/01/11 - 12/31/11		01/01/12 - 03/30/12		04/01/12 - 06/30/12		07/01/12-09/30/12	
Q9	Cumulative Total	Q10	Cumulative Total	Q11	Cumulative Total	Q12	Cumulative Total
$65,395	$850,732.00	$65,395	$916,127.00	$ 65,395.00	$981,522.00	$0.00	$981,522.00
$31,569	$358,364.00	$31,570	$389,934.00	$ 31,570.00	$421,504.00	$0.00	$421,504.00
$96,964.00	$1,209,096.00	$96,965.00	$1,306,061.00	$ 96,965.00	$1,403,026.00	$0.00	$1,403,026.00
$77,738.17	$673,826.64	$41,836.42	$715,663.06	$38,396.10	$754,059.16	$71,422.57	$825,481.73
$59,855.00	$356,435.49	$8,730.93	$365,166.42	$35,423.78	$400,590.20	$0.00	$400,590.20
$137,593.17	$1,030,262.13	$50,567.35	$1,080,829.48	$73,819.88	$1,154,649.36	$65,395.00	$1,220,044.36
-$12,343.17	$176,905.36	$23,558.58	$200,463.94	$26,998.90	$227,462.84	$65,395.00	$292,857.84
-$28,286.00	$1,928.51	$22,839.07	$24,767.58	-$3,853.78	$20,913.80	$31,570.00	$52,483.80
-$40,629.17	$178,833.87	$46,397.65	$225,231.52	$23,145.12	$248,376.64	$96,965.00	$345,341.64

Budget Period 4

		Year 4	Start: 10/1/2012			End: 09/30/2013	
10/01/12 - 12/31/12		01/01/13 - 03/30/13		04/01/13 - 06/30/13		07/01/13-09/30/13	
Q13	Cumulative Total	Q14	Cumulative Total	Q15	Cumulative Total	Q16	Cumulative Total
$0	$981,522.00	$0	$0.00	$ -	$0.00	$0.00	$0.00
$0	$421,504.00	$0	$0.00	$ -	$0.00	$0.00	$0.00
$0.00	$1,403,026.00	$0.00	$1,403,026.00	$ -	$1,403,026.00	$0.00	$1,403,026.00
$128,973.89	$954,455.62	$30,301.85	$984,757.47	$15,448.89	$1,000,206.36	$24,242.86	$1,024,449.22
$0.00	$400,590.20	$473.64	$401,063.84	$0.00	$401,063.84	$123,081.39	$524,145.23
$128,973.89	$1,355,045.82	$30,775.49	$1,385,821.31	$15,448.89	$1,401,270.20	$147,324.25	$1,548,594.45
-$128,973.89	$27,066.38	-$30,301.85	-$984,757.47	-$15,448.89	-$1,000,206.36	-$24,242.86	-$1,024,449.22
$0.00	$20,913.80	-$473.64	-$401,063.84	$0.00	-$401,063.84	-$123,081.39	-$524,145.23
-$128,973.89	$47,980.18	-$30,775.49	$17,204.69	-$15,448.89	$1,755.80	-$147,324.25	-$145,568.45